## Title
Self-Assembled p-Carborane Analogue of p-Mercaptobenzoic Acid on Au{111}



## Journal
Chemistry of Materials, 27(15)

## ISSN
0897-4756

## Authors
Thomas, John C
Boldog, Ishtvan
Auluck, Harsharn S
et al.

## Publication Date
2015-08-11

## DOI
10.1021/acs.chemmater.5b02263

Peer reviewed

cm CHEMISTRY OF MATERIALS

AUGUST 11, 2015 | VOLUME 27 | NUMBER 15 | pubs.acs.org/cm

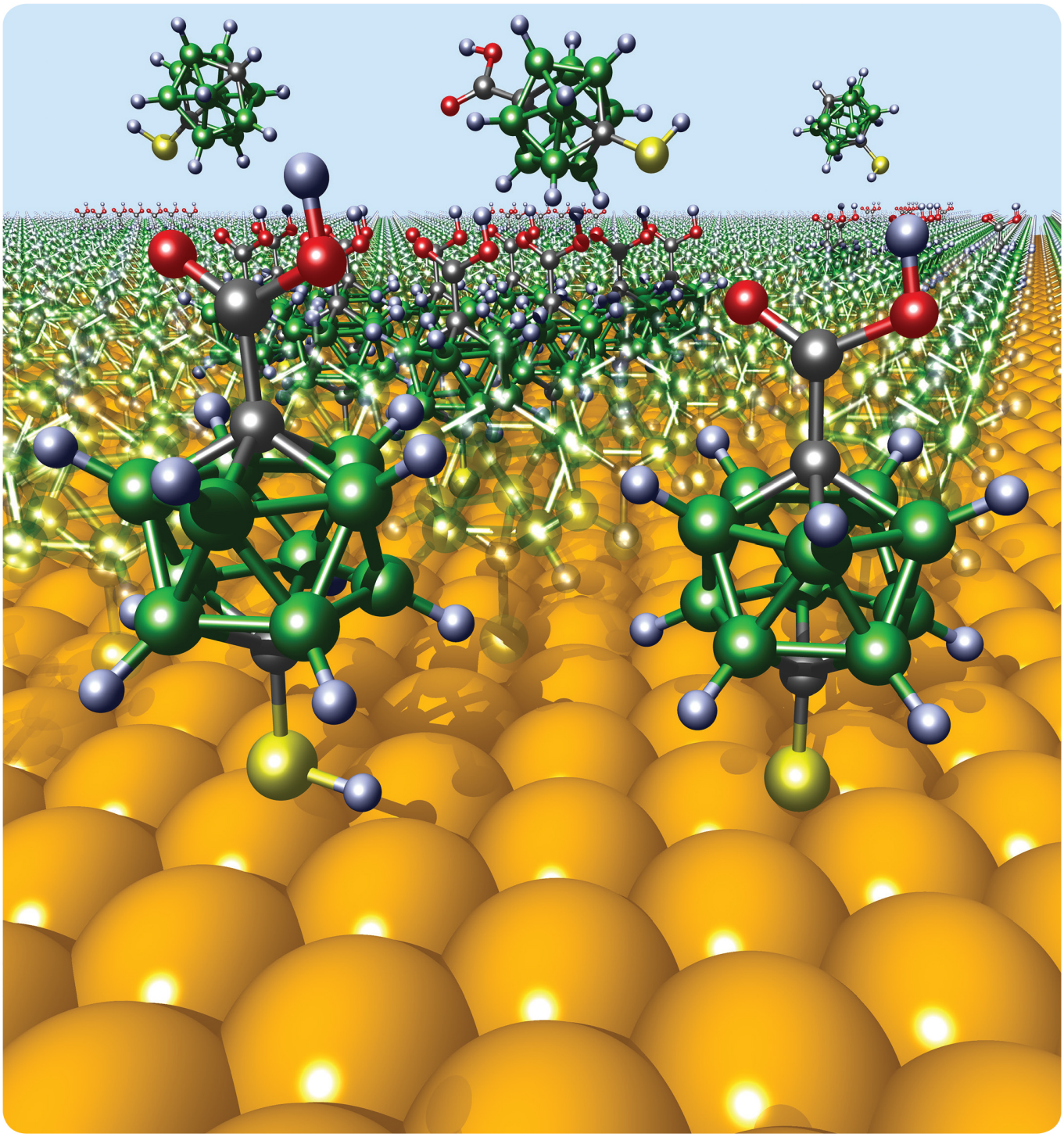

ACS Publications
Most Trusted. Most Cited. Most Read.

www.acs.org

CHEMISTRY OF MATERIALS

Article

pubs.acs.org/cm

# Self-Assembled *p*-Carborane Analogue of *p*-Mercaptobenzoic Acid on Au{111}

John C. Thomas,[†] Ishtvan Boldog,[‡] Harsharn S. Auluck,[†] Pablo J. Bereciartua,[⊥] Michal Dušek,[⊥] Jan Macháček,[‡] Zdeněk Bastl,*[,§] Paul S. Weiss,*[,†,∥] and Tomáš Baše*[,‡]

[†]Department of Chemistry and Biochemistry and California NanoSystems Institute, University of California, Los Angeles, Los Angeles, California 90095, United States

[‡]Institute of Inorganic Chemistry, Academy of Sciences of the Czech Republic, v.v.i. 250 68 Husinec-Řež, č.p. 1001, Czech Republic

[⊥]Institute of Physics, Academy of Sciences of the Czech Republic, Na Slovance 1999/2, 182 21 Prague 8, Czech Republic

[§]J. Heyrovský Institute of Physical Chemistry, Academy of Sciences of the Czech Republic, v.v.i. Dolejškova 3, 182 23 Prague 8, Czech Republic

[∥]Department of Materials Science and Engineering, University of California, Los Angeles, Los Angeles, California 90095, United States

Supporting Information

**ABSTRACT:** The *p*-carborane cluster analogue of *p*-mercaptobenzoic acid, 1-HS-12-COOH-1,12-$C_2B_{10}H_{10}$, has been synthesized and characterized using nuclear magnetic resonance spectroscopy, single-crystal X-ray diffraction analysis, quantum-chemical calculations, and scanning tunneling microscopy. The single-crystal structure and selected packing aspects are discussed and presented in comparison with the two-dimensional periodic arrangements. Scanning tunneling micrographs, recorded under ambient conditions, are used to compare pure monolayers of 1-HS-1,12-$C_2B_{10}H_{11}$ to coadsorbed monolayers of both the parental precursor and carboxyl-functionalized *p*-carboranethiolate on Au{111}. Monolayers of both constituents are further characterized by X-ray photoelectron spectroscopy, which shows good agreement between the stoichiometry of each pure monolayer and the nominal stoichiometries of the respective molecules. Results indicate that most of the molecules of both derivatives adsorb as thiolates but that a small fraction of each adsorbs as thiols, without complete SH bond scission, and consequently are labile relative to desorption. Wetting-angle measurements confirm the hydrophilic character of monolayers containing the carboxylic acid constituents. Mixed self-assembled monolayers with functionalized constituents of high axial symmetry provide a convenient basis for grafting two- and three-dimensional structures.

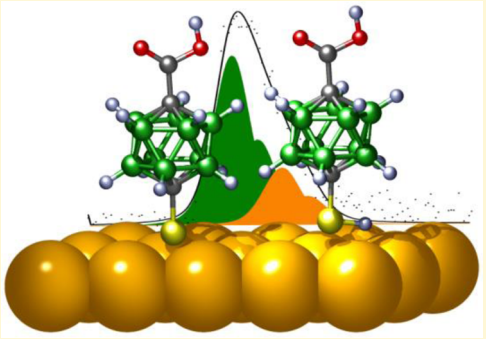

## INTRODUCTION

Self-assembled monolayers (SAMs), or pseudo-crystalline two-dimensional (2D) interfaces, enable tunable surface properties that find use in nanotechnology and materials development applications.[1,2] Functionalization of molecules used as essential building blocks for SAMs is a target in efforts to understand and to control materials at the molecular level and to use individual molecules for the preparation of bottom-up surface assemblies with tailored dimensions, physicochemical properties, and chemical compositions.[3,4] The most common two-dimensional (2D) assemblies comprise organic molecules tethered to gold surfaces via thiol (-SH)/thiolate ($-S^-$) anchoring groups.[5] Recently, in this context, cage molecules have attracted special attention because of their rigid three-dimensional (3D) architectures and extraordinary capacity for structural and chemical modifications.[6−13] Thiolated derivatives of 12-vertex dicarba-*closo*-dodecaboranes of the general formula $(HS)_x$-$C_2B_{10}H_{12-x}$, with their nearly regular icosahedral molecular structures, are representatives of inorganic cluster molecules belonging to this category.[14−16] They have been used as essential components of self-assembled monolayers and have been shown to possess several advantages compared to their organic counterparts, such as higher stability against heating and chemical substitution and pristine monolayer formations that have fewer types and total numbers of defects.[17,18] The latter advantage can be ascribed to the higher axial isotropy of the carborane-based backbones compared to the organic aromatic varieties; this fundamental difference stimulates our research. The large dipole moments in different isomeric carboranethiols enable tunable effective work function modification over a variety of coinage metal substrates.[2,19−21] These robust molecules have also been embedded in functional organic-based SAMs due to their steric properties and wide frontier−orbital energy gaps.[8,22]

Received: June 15, 2015
Published: June 24, 2015





DOI: 10.1021/acs.chemmater.5b02263
*Chem. Mater.* 2015, 27, 5425−5435

Recently, new synthetic strategies for the preparation of the dicarba-*closo*-dodecaborane derivatives substituted at both carbon and boron positions have been proposed as pathways to new precursors and ligands for metal surfaces and coordination compounds.[23−25] These efforts reflect a systematic approach toward forming a library of functionalized carborane cluster compounds with potential use as surface modifiers with new qualities. Our focus is to probe the library of potential carborane-based building blocks in the context of SAMs with importance in supramolecular and materials chemistry through targeted functionalization. These SAM constituents are interesting for ultrathin film applications, and thus functionalized *p*-isomers become intriguing options for directing nanoarchitectures from two dimensions into three.[2,7,9,16,26]

In this study, we report on the preparation and characterization of a new cage-thiol with a carboxylic functional group suitable for further chemical modification on exposed self-assembled monolayer surfaces. Our attempt to prepare and to investigate the cluster analogue of *p*-mercaptobenzoic acid (1-HS-4-COOH-$C_6H_4$) as a modifier of gold surfaces was inspired by recent successes in functionalizing and patterning with *p*-mercaptobenzoic acid itself,[27−31] which has proven to be effective for surface functionalization. The new cage-molecule building block, 1-HS-12-COOH-1,12-$C_2B_{10}H_{10}$ (**A′**), has high axial symmetry, which is another reason for our interest in its use for SAMs. In comparison to the benzene ring of *p*-mercaptobenzoic acid, the larger steric demands of the carborane cage enable greater separations of the carboxylic functional groups in two dimensions. Particularly attractive is the potential use of this new carborane derivative as a functional capping ligand for gold colloidal particles or as a ligand for transition metal complexes. We compare its structure to that of its precursor 1-HS-1,12-$C_2B_{10}H_{11}$ (**A**) as the first step for examination, where single-crystal packing data from X-ray diffraction analysis are discussed and compared to micrographs obtained by scanning tunneling microscopy (STM). The nature of these two SAM constituents on gold surfaces has been quantified by X-ray photoelectron spectroscopy (XPS) and contact angle measurements that demonstrate the surface wetting characteristics.

## RESULTS AND DISCUSSION

**Synthesis, Nuclear Magnetic Resonance Spectroscopic Characterization, and X-ray Structural Analysis.** 1-Mercapto-1,12-dicarba-*closo*-dodecaborane-12-carboxylic acid (**A′**) was synthesized from 1-mercapto-1,12-dicarba-*closo*-dodecaborane (**A**) by lithiation with two equivalents of *n*-BuLi and subsequent reaction with carbon dioxide followed by quenching with an aqueous solution of hydrochloric acid (Scheme 1).

This new derivative is an inorganic cage analogue of *p*-mercaptobenzoic acid. $^{11}B$, $^{1}H$, and $^{13}C$ nuclear magnetic resonance (NMR) spectra of the new compound were measured, and all resonances were assigned to the respective atoms (Table 1). The molecular structure of **A′** was obtained from a single-crystal X-ray diffraction analysis; see Figure 1. In the NMR data, we note that the thiol proton chemical shift in **A′** of 3.18 ppm practically does not differ from the value of 3.19 ppm measured in **A**. It demonstrates that the *p*-carborane cage effectively isolates both functional groups.

Single-crystal X-ray diffraction study of **A′** established the positions of all the heavier atoms in the molecules. All cluster

**Scheme 1. Synthesis of 1-HS-12-COOH-1,12-$C_2B_{10}H_{10}$ (A′) Starting from the Parental 1-HS-1,12-$C_2B_{10}H_{11}$ Precursor (A)**

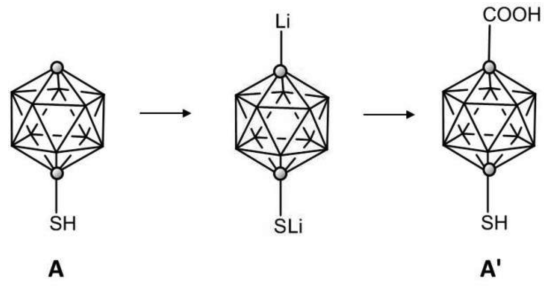


hydrogen atoms were apparent in the residual electron-density map after anisotropic refinement of the heavier atoms. After isotropic refinement of all cluster hydrogen atoms, the remaining highest residual electron density peaks revealed the thiol and carboxyl hydrogen atoms. The thiol hydrogen atoms showed crystallographic disorder that is discussed below.

1,12-Dicarba-*closo*-dodecaborane (1,12-$C_2B_{10}H_{12}$) exhibits contraction along the C···C axis of the molecule and shows the *d*[C(1)···C(12)] of 3.056(6) Å.[32] This shorter distance compared to the antipodal B···B distances, Ø 3.377(6) Å, which are similar to the *d*[B(1)···B(12)] of 3.383(2) Å[33] in $[B_{12}H_{12}]^{2-}$, expresses the extent to which the structure deviates from the geometry of a regular icosahedron.

Different substituents attached to the carbon atoms have an additional effect on the C(1)···C(12) distance as a consequence of their electronic influence. The SH group represents an electronegative substituent that pulls electrons from the cluster carbon atoms and causes elongation of the C(1)···C(12) distance. A good example is the structure of 1,12-$(HS)_2$-1,12-$C_2B_{10}H_{10}$ that has been previously investigated using single-crystal X-ray diffraction[19] and gas-phase electron diffraction (GED)[34] and by means of computational analyses.[19,34] Table 2 shows two mutually related cluster parameters: the C(1)···C(12) distance and the angle $\alpha$ that are both defined in Figure 1. The molecule of **A′** exhibits the *d*[C(1)···C(12)] of 3.091(3) Å, which is slightly shorter than the d[C(1)···C(12)] of 3.107(3) Å in 1,12-$(HS)_2$-1,12-$C_2B_{10}H_{10}$. The COOH functional group elongates the C(1)···C(12) distance less than the SH group. Since neither the molecule **A′** nor **A** has perfect $D_{5d}$ symmetry, the parameter $\alpha$ represents the average value. We distinguish in Table 2 between angle $\alpha_{COOH}$ and $\alpha_{SH}$ reflecting whether the value belongs to the pentagonal pyramid close to the SH or COOH group. Similarly, two angles ($\alpha_{SH}$ and $\alpha_{H}$) are distinguished for the calculated structure of **A**, which has an SH group attached to only one of the carbon atoms, while the other bears hydrogen as in the unsubstituted 1,12-dicarba-*closo*-dodecaborane, 1,12-$C_2B_{10}H_{12}$.

Additional analyses of the interatomic distances in both **A** and **A′**, such as B−B connections, show that the cluster does not exhibit any other significant changes due to the presence of the thiol (-SH) or carboxyl (−COOH) substituents than those reported above. With respect to these findings, the cluster architecture can be more precisely described as a bicapped pentagonal antiprism.

The supramolecular structure of **A′**, as it appears in the single crystal, is depicted in Supporting Information Figure S1. It consists of molecular pairs bound in the typical dimeric $R_2^2(8)$ association pattern[35] of carboxylic acids with the O···(H)···O


DOI: 10.1021/acs.chemmater.5b02263
*Chem. Mater.* 2015, 27, 5425−5435

**Table 1. Measured $^{11}B$, $^{13}C$, and $^{1}H$ NMR Chemical Shift Data for Compounds 1-HS-12-COOH-1,12-$C_2B_{10}H_{10}$ (A′) and 1-HS-1,12-$C_2B_{10}H_{11}$ (A) in $CD_3OD$ Solution at 300 K**

| | A′ | | | A | | |
|---|---|---|---|---|---|---|
| assign. | $\delta$ $^{11}B$ | $\delta$ $^{1}H$ | $\delta$ $^{13}C$ | $\delta$ $^{11}B$ | $\delta$ $^{1}H$ | $\delta$ $^{13}C$ |
| 1 | | | 74.07 | | | 74.56 |
| 2−6 | −11.25 | 2.41 | | −10.22 | 2.45 | |
| 7−11 | −13.20 | 2.47 | | −14.09 | 2.19 | |
| 12 | | | 72.69 | | 3.14 | 58.30 |
| S-*H* (1) | | 3.18 | | | 3.19 | |
| *COO-H* (12) | | 3.74[a] | 163.21 | | | |

[a]The respective proton appears as a broad band.

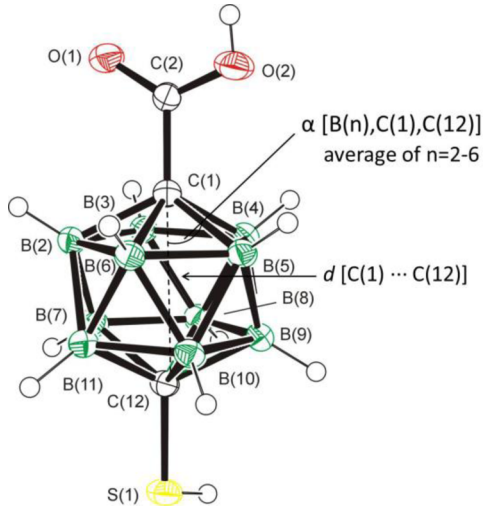


**Figure 1.** Crystallographically determined molecular structure of 1-HS-12-COOH-1,12-$C_2B_{10}H_{10}$ (**A′**).

**Table 2. Selected Cluster Geometry Parameters for Compounds 1-HS-12-COOH-1,12-$C_2B_{10}H_{10}$ (A′), 1-HS-1,12-$C_2B_{10}H_{11}$ (A), and for Comparison also 1,12-$(HS)_2$-1,12-$C_2B_{10}H_{10}$, 1,12-$C_2B_{10}H_{12}$, and $[B_{12}H_{12}]^{2-}$**

| | $\alpha$,[a] deg | $d$[C(1)···C(12)],[a] Å |
|---|---|---|
| **A′** | 62.4(1)$^{sc,\alpha(COOH)}$ | 3.091(3)$^{sc}$ |
| | 62.2(1)$^{sc,\alpha(SH)}$ | |
| | 62.43$^{comp,\alpha(COOH)}$ | 3.077$^{comp}$ |
| | 62.15$^{comp,\alpha(SH)}$ | |
| **A** | 62.18$^{comp,\alpha(SH)}$ | 3.067$^{comp}$ |
| | 62.74$^{comp,\alpha(H)}$ | |
| 1,12-$(HS)_2$-1,12-$C_2B_{10}H_{10}$ | 62.0(1)$^{sc,19}$ | 3.107(3)$^{sc,19}$ |
| | 62.15$^{comp,19}$ | 3.091$^{comp,19}$ |
| 1,12-$C_2B_{10}H_{12}$ | 62.8(2)$^{sc,32}$ | 3.056(6)$^{sc,32}$ |
| $[B_{12}H_{12}]^{2-}$ | 58.3(1)$^{sc,33}$ | 3.383(2)$^{sc,33,b}$ |

[a]Superscript sc: data from an X-ray structural analysis of a single crystal; superscript comp: computational data. [b]$d$[B(1)···B(12)].

interatomic distance of 2.647 Å. In contrast, the thiol groups facing each other form a zigzag arranged $-(SH)_n-$ chain, along the lattice vector *a*, with the S···(H)···S interatomic distances between 4.002 and 4.057 Å. The hydrogen atoms within the $-(SH)_n-$ chains are crystallographically disordered (Supporting Information Figure S2). **A′** is soluble in most polar as well as nonpolar organic solvents, and it is worth noting that these molecules might exist, especially in aprotic solvents, in the form of the nondissociated dimers.

In the direction along the $-(SH)_n-$ chain, perpendicular to the C(1)···C(12) axis of the molecules, the cages are arranged in rows with nearest-neighbor distances of 6.635 Å. Figure 2

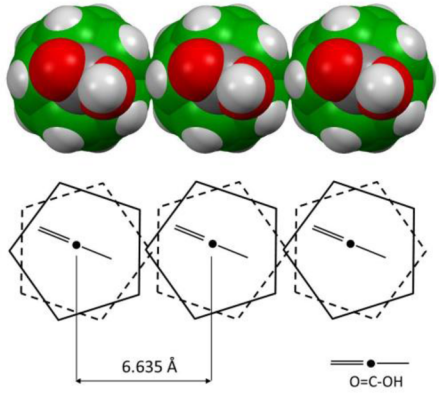


**Figure 2.** Space-filling (top) and schematic (bottom) drawings of a part of the crystallographic structure of **A′** (viewed along the C(1)···C(12) vectors of the molecular structure, with COOH groups on top) illustrating the closest packing of the molecules in a single crystal.

shows space-filling and schematic drawings of this row with COOH groups on top, which illustrate how close this nearest intermolecular distance is compared to the intermolecular distance in a SAM.

Another important note is the alignment of the COOH groups that are, in a crystal structure, involved in strong hydrogen-bonding interactions between two COOH groups and contribute significantly to the crystal packing forces. This hydrogen bond does not occur in a SAM. Independent analyses of the COOH group conformation were done using MP2/6-31+G* calculations. Two conformations (Figure 3) were investigated, and the −COOH rotational barrier was assessed. Computational data show almost free rotation of the COOH group, which may contribute to difficulties in obtaining molecular resolution with STM (vide infra). The distance between two molecules on a flat surface precludes any significant direct lateral hydrogen-bonding interactions between the COOH groups. Figure 3 shows a schematic of two potential conformations denoted as 0° and 180° according to the B—C—C═O torsion angle. The difference between the alignment of COOH groups in the crystal structure and the computational analyses is attributed to almost free rotation of the COOH groups, assessed from the energy barrier, and to the effect of crystal packing forces.

In the computationally optimized geometries of 1-($S^-$)-12-COOH-1,12$C_2B_{10}H_{10}$, the SH hydrogen atom was removed



DOI: 10.1021/acs.chemmater.5b02263
*Chem. Mater.* 2015, 27, 5425−5435

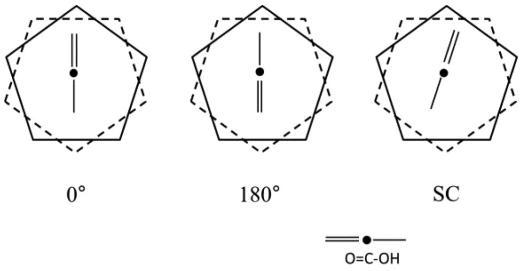


**Figure 3.** Schematic representation of two computationally optimized −COOH conformations (0° and 180°) and the conformation observed in single crystals (SC). The black dot in the middle indicates the position of a COOH carbon atom. The double line represents the doubly bonded oxygen, and the single line represents hydroxyl part of the carboxylic group.

intentionally for reasons of simplicity. The conformation with the doubly bonded oxygen of the carboxyl group over a B−B connection line and its hydroxyl over a boron atom (conformation 180°) is the most stable one, while the opposite (conformation 0°), with the doubly bonded oxygen over a boron and the hydroxyl over a B−B connection line, has the highest energy.

The barrier of the carboxyl rotation is nevertheless small, 0.00345 eV at the HF/6-31+G* level, which becomes 0.00149 eV with zero-point correction and 0.00210 eV at the MP2/6-31+G* level (without zero-point correction). At the laboratory temperature of 20 °C, it is significantly smaller than the thermal energy, kT = 0.0253 eV, which is expected to lead to essentially unrestricted rotation. These computational results are summarized in the Supporting Information (Table S2).

The packing of molecules in single crystals as well as different structural aspects of the molecule itself offer an opportunity for comparison with the packing in a self-assembled monolayer on Au{111}.

**Scanning Tunneling Microscopy.** We first imaged 2D lattices of **A** on Au{111}/mica with molecular resolution under ambient conditions and used this lattice as a backbone to trap islands of **A′** in mixed (1:10, **A′**:**A**) deposited SAMs. Single-component SAMs of **A′** were difficult to visualize with molecular resolution under ambient conditions due to strongly hydrophilic COOH functional groups that rotate almost freely around the fivefold symmetry axis of the *p*-carborane cage and are likely to adsorb water.

We use STM as a tool to probe the exposed interfaces of conductive thin films with molecular precision.[36,37] Constant-current mode imaging was used to acquire data that represent a convolution of topography and electronic structure.[38,39] Homogenous monolayers of **A** on Au{111} form into two-phase hexagonally close-packed arrays with a 7.2 ± 0.5 Å nearest neighbor spacings (Figure 4 and Supporting Information Figure S3), consistent with our earlier measurements of SAMs of simple carboranethiols on Au{111}.[18] This spacing is greater than the closest arrangement observed in the crystal structure (Figure 2). Possible unit cell structures include $(\sqrt{97} \times \sqrt{97})R15.30°$, (5 × 5), $(\sqrt{57} \times \sqrt{57})R6.59°$, and $(\sqrt{7} \times \sqrt{7})R19.12°$ which have nearest-neighbor spacings of 7.09, 7.2, 7.25, and 7.62 Å, respectively. Measured SAMs may compete between any of the above structures; incommensurate lattices are also possible.[40,41]

Simple calculations of a 2D array of **A**, used to estimate the steric demands of the cage moiety, predict nearest-neighbor intermolecular distances of 7.26 Å (Figure 5), which best fits the $(\sqrt{57} \times \sqrt{57})R6.59°$ unit cell structure.

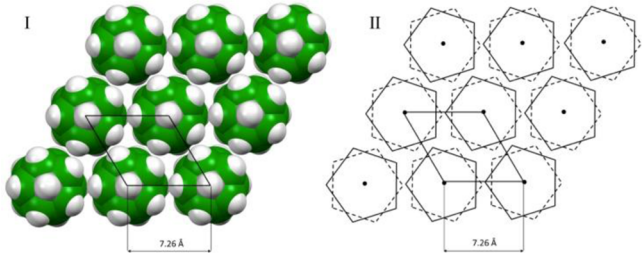


**Figure 5.** Calculated (using density functional theory) 2D array of molecules **A** showing a close-packed structure with the lattice parameters 7.26 Å × 7.27 Å (α = 60.07°). Space-filling (**I**) and schematic (**II**) representations.

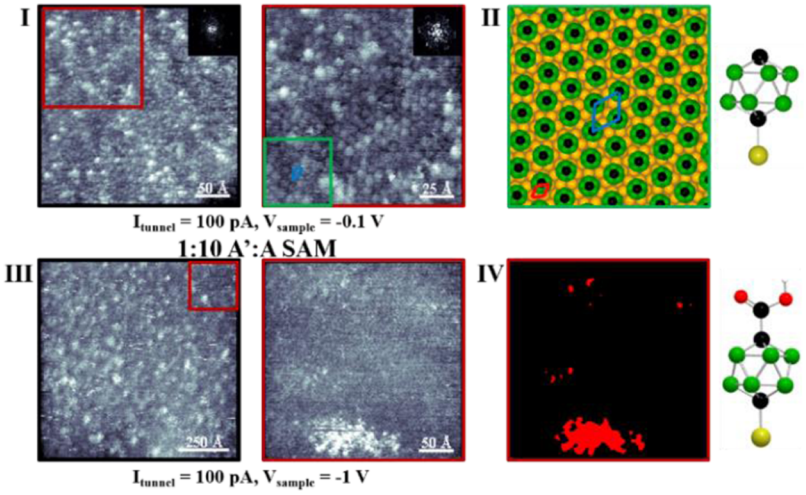


**Figure 4.** (I) Scanning tunneling micrographs ($I_{tunneling}$ = 100 pA, $V_{sample}$ = −0.1 V) of **A** at 280 Å × 280 and 140 Å × 140 Å. Each inset depicts a Fourier transform showing a hexagonally close-packed array with nearest-neighbor spacings of 7.2 ± 0.5 Å. (II) Structural schematic depicting the observed lattice (blue lines indicate nearest neighbors) with respect to the underlying (1 × 1) unit cell (red rhombus) of the unreconstructed Au{111} substrate. (III) Scanning tunneling micrographs ($I_{tunneling}$ = 100 pA, $V_{sample}$ = −1.0 V) of a codeposited (1:10, **A′**:**A**) SAM, at both 940 Å × 940 and 280 Å × 280 Å scan sizes. (IV) Thresholding enables the isolation of **A′** regions that are highlighted in red.



DOI: 10.1021/acs.chemmater.5b02263
*Chem. Mater.* 2015, 27, 5425−5435

The five-fold symmetry of the *para*-carborane cage precludes the calculated lattice constants from being the same. Two phases that differ in apparent height ($dz_{apparent}$ = 1.0 ± 0.3 Å) were measured. We attribute the lower apparent height features to thiolate-bound moieties and the more protruding apparent height features to thiol moieties. Local analyses across different areas and samples ($n_{samples}$ > 3) exhibit an average coverage of 5.1 ± 1.4% of the thiol-bound moiety and a 95 ± 3% average coverage of the thiolate-bound moiety (Supporting Information Figure S4), indicating that the thiolate bound state is preferred and dominant. In this regard, it is important to note that previous STM investigations of the isomeric 1-HS-1,7-$C_2B_{10}H_{11}$ showed only the thiolate-bound state.[18] This mixed composition SAM proved useful in promoting sparse **A′** monolayer formation. Scanning tunneling micrographs of codeposited SAMs show distributed islands of **A′**, where the lattice of the **A** backbone is confirmed and **A′** is resolved in apparent height. Hydrogen bonding among the molecules of **A′** in solution may play a major role in its 2D packing, due to intermolecular forces, and thus the formation of island aggregates. Scanning tunneling micrographs show a difference in apparent height of 1.2 ± 0.2 Å, under the conditions used, where the carboxyl moiety is topographically more protruding (Supporting Information Figure S5). Local ordering of the **A** backbone, with minimal defects surrounding **A′** patches, suggests the **A′** moieties have adopted the same nearest neighbor spacing as the backbone monolayer of ∼7.2 Å, as has been observed in other SAMs.[37] This system may find use in the preparation of patterned substrates with chemically functionalized island targets dispersed within monolayer matrices.[1,16,30,42−51]

**X-ray Photoelectron Spectroscopy.** X-ray photoelectron spectroscopy (XPS) was used to investigate the adsorption of both derivatives, **A** and **A′**, on Au{111} surfaces further. The respective data are summarized in Tables 3 and 4. Good agreement between the measured and nominal stoichiometries of the molecules was observed.

**Table 3. Atomic Concentrations of Elements on Au Surfaces Modified with A and A′ Compounds Relative to the Concentration of Boron Atoms (=10) As Determined from XPS Analyses Assuming Homogeneous Samples[a]**

| sample[b] | S | $C_{CB(CO)}$ | $C_{CH,CC}$[c] | $C_{CO}$ | Au | O |
|---|---|---|---|---|---|---|
| **A** | | | | | | |
| Au{111}$^{s}$ | 1.1 | 2.0 | 1.4 | ∼0 | 20.0 | 0.9 |
| Au{111}$^{gp}$ | 1.1 | 2.0 | 2.7 | 0.6 | 10.8 | 1.4 |
| **A′** | | | | | | |
| Au{111}$^{s}$ | 1.0 | 2.7 | 2.5 | 1.2 | 10.7 | 4.5 |
| 350 °C | 1.2 | 3.8 | 7.4 | 0.8 | 29.0 | - |
| Au{111}$^{gp}$ | 1.2 | 2.4 | 5.4 | 1.0 | 28.0 | 2.3 |

[a]Au is included as a relative measure of the surface coverage by the adsorbed species; higher Au signals indicate lower carborane coverages. [b]Superscript s: adsorption from solution; superscript gp: adsorption from the gas phase. [c]Adventitious carbonaceous contamination.

The XPS data provide important information about the form in which the molecules are adsorbed on gold surfaces (**A** SAM and **A′** SAM). Of particular use in this respect are the binding energy (BE) values of S 2p electrons summarized in Table 4.

Both derivatives **A** and **A′** self-assembled on Au{111} show comparable spectra in the S 2p region with sulfur atoms in two

**Table 4. Measured Core-Level Binding Energies and FWHM[a] (parentheses) for Au Films Modified with 1-HS-1,12-$C_2B_{10}H_{11}$ (A) and 1-HS-12-COOH-1,12-$C_2B_{10}H_{10}$ (A′)[b]**

| sample[c] | S $2p_{3/2}$ | B 1s | C 1s |
|---|---|---|---|
| **A** | | | |
| Au{111}$^{s}$ | 162.1 (2.0) | 189.1 (1.9) | 284.4 (2.1) |
| | 164.0 (2.0) | | 285.9 (2.1) |
| Au{111}$^{gp}$ | 162.5 (2.2) | 189.1 (1.9) | 284.6 (2.2) |
| | 164.6 (2.2) | | 286.2 (2.2) |
| | | | 289.0 (2.2) |
| **A′** | | | |
| Au{111}$^{s}$ | 162.2 (1.8) | 189.2 (2.1) | 284.7 (2.2) |
| | 164.0 (1.8) | | 286.1 (2.2) |
| | | | 288.8 (2.2) |
| 350 °C | 162.4 (2.5) | 189.7 (2.2) | 284.5 (2.4) |
| | | | 286.0 (2.4) |
| | | | 288.7 (2.4) |
| Au{111}$^{gp}$ | 161.9 (2.2) | 189.1 (1.9) | 284.5 (2.2) |
| | 164.1 (2.2) | | 286.1 (2.2) |
| | | | 289.0 (2.2) |

[a]Full width at half-maximum. [b]The binding energy of Au $4f_{7/2}$ is 84.0 eV for all samples. All values are in eV. [c]Superscript s: adsorption from solution; superscript gp: adsorption from the gas phase.

oxidation states and the amount of the second component ranging from 12% to 39% (Figure 6). The COOH group does not show any evident influence on how these two derivatives adsorb on the surface.

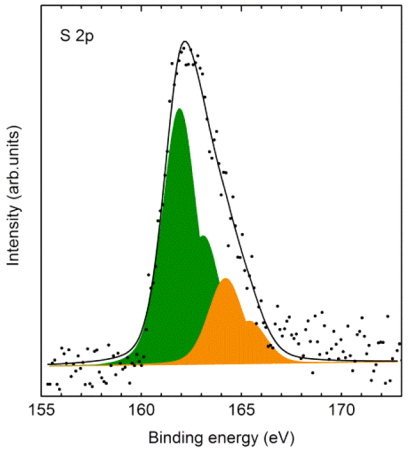


**Figure 6.** X-ray photoelectron spectrum of S 2p photoelectrons fit to indicate the contributions of both the thiolate (green) and the thiol (yellow) bound moieties of A′ on Au{111} (background subtracted).

This observation corresponds to practically identical S−H proton chemical shifts in $^1$H NMR spectra of both **A** and **A′** (Table 1). The measured BE value of S $2p_{3/2}$ electrons at ∼162.0 eV is comparable to the value reported in the literature[52−54] for alkanethiolates on planar gold surfaces. The second sulfur species with the S $2p_{3/2}$ electrons at ∼164 eV can be assigned to a free thiol (−SH) group.[52−54] Observations of sulfur atoms in both states can be rationally explained by a fraction of molecules being adsorbed on the Au{111} surface without SH bond scission. The BE value of the second


DOI: 10.1021/acs.chemmater.5b02263
*Chem. Mater.* 2015, 27, 5425−5435

component assigned to the thiol moiety interacting with a Au{111} surface, ~164.0 eV, is close to 163.7 eV, which was reported previously for a free SH group in 1,12-$(HS)_2$-1,12-$C_2B_{10}H_{10}$.[19] This small, reproducible difference can be understood by the interaction of the lone pair electrons of sulfur of the nondissociated SH group with a gold surface, which reduces the electron density on the S atom and thus shifts the BE of S $2p_{3/2}$ electrons to a slightly higher value. We note that we do not have information from the STM images nor the XPS data on any possible reorganization of Au substrate atoms. Evidence for Au adatom and so-called staple structures have been observed in a number of studies of alkanethiols, alkaneselenols, and related molecules on Au{111} and on nanoparticle surfaces.[10,37,55−60] Heating the SAM of **A′** on Au{111} up to 350 °C in the X-ray photoelectron spectrometer led to the disappearance of the (protonated) sulfur with the binding energy value of ~164.0 eV, and was accompanied by a corresponding decrease of the surface concentration of carborane molecules and an increase of the signal from the gold substrate (Tables 3 and 4). This result points to the (expected) higher thermal stability of the thiolate form of the molecules in the SAM.

By this means, one can tune the ratio of thiolate and thiol molecules on the surface. This observation is consistent with the STM analyses of the SAMs prepared at higher temperatures, which exhibit lower surface fractions of the features that we attribute to the adsorbed thiol (i.e., protonated) moiety. Thus, temperature provides a means for controlling the surface ratio of these species both on deposition and via subsequent processing. The former provides a complete monolayer whereas later heating is expected to enable access to the substrate and thus to open up space for further deposition.[31]

An alternative preparation of the SAMs is from their constituent vapors (in this report referred to as gas phase, GP, adsorption).[61,62] This strategy usually leads to less carbon contamination than deposition from solution as the surface is not exposed to solvent. While the spectra of S 2p photoelectrons were in good agreement for both **A** and **A″** SAMs, the surface exposed to the former derivative shows higher coverage, presumably because of the higher volatility of **A** compared to **A′**. In Table 3, the atomic concentration of Au is included as a relative measure of surface coverage.

The spectra of C 1s photoelectrons were fit by three components of the same width with binding energies 284.6, 286.0, and 288.8 eV, which can be assigned to carbon atoms in C−C, C−H (first component), C−B with contribution of C−O (second component), and COO (third component) bonds. As expected, the third component was not present for the adsorbed molecules of **A**. The samples were prepared and transferred under ambient conditions, and consequently some amount of carbonaceous contamination was present on their surfaces.

**Dynamic Contact Angles.** The measurements of dynamic contact angles provide macroscopic characterization of modified surfaces and information about the hydrophilic/hydrophobic surface character.[7,63] Au{111} surfaces modified with derivatives **A** and **A′** show advancing and receding wetting angle values of 87.5 (0.3)° and 76.8 (0.2)° for SAMs of **A**, respectively, and 30.0 (0.1)° and 24.8 (0.1)° for SAMs of **A′**, respectively. The measured values are significantly different and demonstrate the hydrophilic character of SAMs of **A′** compared to those of **A**. The hydrophilic character of SAMs of **A′** is an expected result of the introduction of the exposed COOH functional groups. This result is also consistent with the expected orientations of the molecules on gold surfaces, i.e., with the thiol/thiolate groups anchoring the molecules to the substrate; the carboxylic functional groups interact only weakly with the underlying gold surface and are at the exposed surface. Moreover, both derivatives **A** and **A′** exhibit features in the S 2p region of the XP spectra, and it is therefore unlikely that the second sulfur species, observed at 164.0 eV, would result from the adsorption of **A′** via its carboxylic group.

**Acid−Base Titration of Selected Carboranethiol Derivatives.** The adsorption of **A** and **A′** on Au{111} shows coexisting thiolate- and thiol-bound moieties. This phenomenon has not been observed with closely related species—isomeric to **A**—studied previously with XPS (1-HS-1,2-$C_2B_{10}H_{11}$)[17] and STM (1-HS-1,7-$C_2B_{10}H_{11}$).[18] Therefore, the acidity of the SH group, which is influenced by decreasing electron-accepting properties of the carboranyl backbone in the order from *ortho* through *meta* to *para* isomers, is further analyzed as an intrinsic property of the molecule, determining the thiol (−SH)/thiolate ($-S^-$) adsorption scheme. All derivatives were titrated with aqueous solution of sodium hydroxide and the titration curves are shown with the respective p$K_a$ values in Figure 7. The results show that the

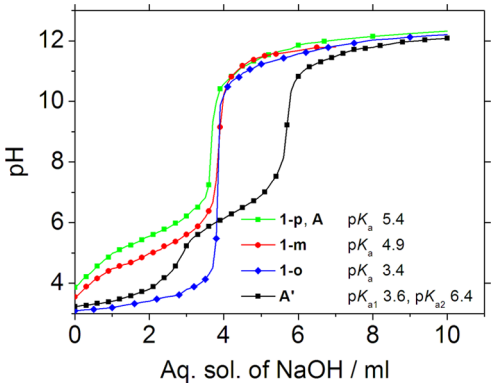


**Figure 7.** Acid−base titration curves of 1-HS-1,2-$C_2B_{10}H_{11}$ (**1-o**), 1-HS-1,7-$C_2B_{10}H_{11}$ (**1-m**), 1-HS-1,12-$C_2B_{10}H_{11}$ (**1-p**, **A**), and 1-HS-12-COOH-1,12-$C_2B_{10}H_{10}$ (**A′**).

derivative **A′** is a diprotic acid. Dissociation of the COOH group prior to the SH group is in accord with the acidity constant order, and corresponds to our computational results at the CC2/def2-TZVP level of theory. Comparisons of **A** (1-HS-1,12-$C_2B_{10}H_{11}$) with its positional isomers derived from *ortho*-dicarba-*closo*-dodecaborane, 1-HS-1,2-$C_2B_{10}H_{11}$, and *meta*-dicarba-*closo*-dodecaborane, 1-HS-1,7-$C_2B_{10}H_{11}$, show a trend of increasing SH group acidic character from *para*- through *meta*- to *ortho*-carborane, which is generally expected and confirmed by measured acidity constants. These results are in good agreement with previously published constants[64] and also are consistent with our computational results, presented in Figure 8. Of the three isomers, **A** (1-HS-1,12-$C_2B_{10}H_{11}$) exhibits the greatest energy difference between its protonated and deprotonated form, which corresponds to the weakest acidic character observed in the titration experiments. In comparison, the isomer 1-HS-1,2-$C_2B_{10}H_{11}$ dissociates more easily, shows the smallest energy difference between its protonated and deprotonated forms, and has been previously reported to exhibit only the thiolate species in acquired X-ray photoelectron spectra.[17] A similar trend is observed with the


DOI: 10.1021/acs.chemmater.5b02263
*Chem. Mater.* 2015, 27, 5425−5435

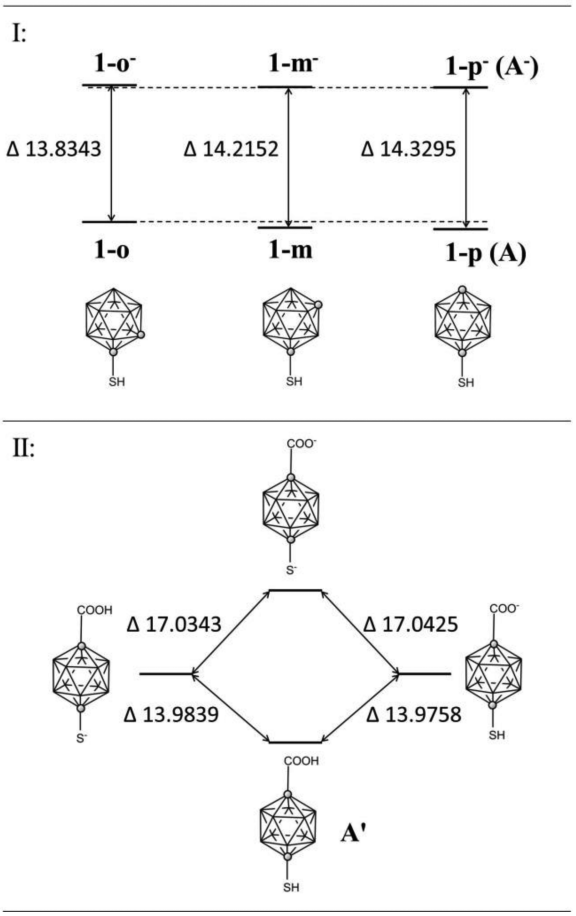


**Figure 8.** (I) Relative energies of 1-HS-1,2-$C_2B_{10}H_{11}$ (**1-o**), 1-HS-1,7-$C_2B_{10}H_{11}$ (**1-m**), 1-HS-1,12-$C_2B_{10}H_{11}$ (**1-p**, **A**), and their respective deprotonated forms (**1-o-**, **1-m-**, and **1-p-**). (II) Relative energies of 1-HS-12-COOH-1,12-$C_2B_{10}H_{10}$ (**A′**) and its deprotonated forms. Schematic representations of the respective molecules are shown without hydrogen atoms in their vertices for clarity. The positions of carbon atoms in the skeletons are marked with circles. All values are in eV.

isomer 1-HS-1,7-$C_2B_{10}H_{11}$ that has been previously reported to show only one apparent height in STM images.

## CONCLUSIONS AND PROSPECTS

A new bifunctional cage molecule, derived from 12-vertex *p*-carborane, for SAMs was synthesized and thoroughly characterized using structural and spectroscopic methods. This new building block has greater steric demands and higher axial symmetry compared to its planar organic analogue, *p*-mercaptobenzoic acid. As a constituent of SAMs on Au{111}, these bulkier molecules arrange into a hexagonal, close-packed array with the nearest-neighbor distance of 7.2 ± 0.5 Å. In single crystals, the molecules assemble into close-packed rows with nearest-neighbor distances of only 6.635 Å. Such tight packing cannot be effectively achieved in a 2D arrangement because no regular 2D periodic pattern can follow the five-fold symmetry axis of the *p*-carborane cage. Both steric demands and axial symmetry, therefore, influence packing on Au{111} surfaces. A mixed SAM of the new constituent and its noncarboxylated analogue shows that this system can be used to prepare pristine monolayers with separated islands of additional functional groups on top, which can be used in targeted surface patterning. The interactions of the new molecule with gold surfaces were investigated by XPS, which shows that the molecules adsorb preferably as thiolates, but a small fraction of bound thiol moieties has also been observed. This result is consistent with previous studies of monothiolated *o*- and *m*-carboranes[17−19] which both dissociate more easily than monothiolated *p*-carborane. The presence of a carboxylic functional group on top of the *p*-carborane is shown to have a negligible effect on the interactions between the SH group and the substrate surfaces.

In comparison with its organic analogue, *p*-mercaptobenzoic acid, **A′** produces SAMs with several interesting properties, mainly resulting from the fact that carborane cages provide more rigid and larger lattice spacings than alkyl or aryl substituents.[7] A large nearest-neighbor spacing and free carboxyl rotation may be further exploited in SAM-modified gold electrodes, where certain proteins exhibit optimal voltammetric responses in mixed alkanethiolate and hydroxyl-terminated alkanethiolate SAM-modified electrodes.[64] Similar modification on the *m*- and *o*-isomers would enable increased backbone interaction strengths primed for surface functionalization.[65] These observations complement the results obtained recently with similar *p*-carborane derivatives used as building blocks for metal−organic frameworks.[41,49] Combinations of both kinds of carborane-based building blocks provide bases for grafting porous 3D structures such as *p*-carboranylcarboxylate metal−organic frameworks.

## EXPERIMENTAL SECTION

**General Procedures and Chemicals.** 1-HS-1,12-$C_2B_{10}H_{11}$ (**A**) was prepared according to the literature,[66,67] and its purity was checked by gas chromatography with mass spectrometric detection (GC-MS) and by $^{11}B$ and $^{1}H$ NMR spectroscopy. Nuclear magnetic resonance spectroscopy was performed at room temperature on a Varian MercuryPlus at 400 MHz using standard techniques and procedures. Acid−base titrations were done according to the procedure reported previously.[68] Dichloromethane (obtained in p.a. grade from Penta a.s., Czech Republic) was additionally dried over anhydrous $K_2CO_3$ for several weeks and freshly distilled prior to use. Monoglyme (1,2-dimethoxyethane) and *n*-BuLi (2.5 M solution in hexanes) were both purchased from Sigma-Aldrich. Monoglyme was additionally dried with sodium in the presence of benzophenone (99.8%, purchased from Sigma-Aldrich) and freshly distilled before experiments. Benzene and other solvents for STM experiments were purchased from Sigma-Aldrich and used as received. The NMR spectra were measured in $CD_3OD$ (99.8% D) as received from Eurisotop.

**Synthesis of 1-HS-12-COOH-1,12-$C_2B_{10}H_{10}$ (A′).** 1,12-Dicarba-*closo*-dodecaborane-1-thiol, **A** (1.058 g, 6 mmol), was placed in a dry, Ar-purged 500 mL flask and dissolved in 180 mL of dry and freshly distilled monoglyme. While cooling the reaction mixture in an ice−water bath, 9.6 mL of 2.5 M *n*-BuLi solution in hexanes (24 mmol) was slowly added over an ∼10 min period. The cooling bath was removed shortly after the addition of *n*-BuLi, and the white suspension was stirred for an additional 1.5 h at room temperature. Afterward, carbon dioxide was bubbled through the stirred slurry for approximately 3 h (stream of ∼1−5 L/h), and the reaction mixture was stirred overnight. The solvent was evaporated to dryness under reduced pressure, and 60 mL of distilled water were added that yielded a colorless, slightly turbid solution that was acidified with a 10% aqueous solution of HCl (pH ∼ 2). The precipitated solid was filtered off, washed generously with distilled water, and dried over $CaCl_2$ in an evacuated desiccator. The crude product, 1.132 g, was sublimed (5−15 × $10^{-2}$ Torr, $T$ = 100−125 °C) and yielded 0.96 g (73%) of a pure white solid product. Single crystals, suitable for X-ray diffraction analysis, were obtained by slow sublimation in a glass ampule sealed under reduced pressure (∼0.1 Torr) and stored at ∼40−60 °C. The


DOI: 10.1021/acs.chemmater.5b02263
*Chem. Mater.* 2015, 27, 5425−5435

product is soluble in organic solvents such as ethanol, methanol, diethyl ether, chloroform, and hexane. The NMR data with peak assignments are provided in Table 1. Single-crystal X-ray diffraction analysis is discussed. The sublimed product was further characterized by mass spectrometry using a Thermo-Finnigan LCQ-Fleet Ion Trap instrument with electrospray (ESI) ionization in the negative ion mode. ESI-MS $m/z$: 440.14 (100%, $[2M - H]^-$), calcd 440.30 for $B_{20}C_6H_{23}O_4S_2$; 220.18 (5%, $[M - H]^-$), calcd 220.14 for $B_{10}C_3H_{11}O_2S_1$; 175.17 (5%, $[M - COOH]^-$), calcd 175.16 for $B_{10}C_2H_{11}S_1$; 461.08 (4%, $[2M - H + Na]^-$), calcd 461.29 for $B_{20}C_6H_{23}O_4Na_1S_2$. Both experimental and calculated isotopic distribution envelopes are shown in Figures S8–S11 in the Supporting Information. Melting point: 197–198 °C. Melting was accompanied by turning brown due to decomposition. Elemental analysis: found, C, 16.34; B, 49.04; S, 14.59; H, 5.47; calculated for $B_{10}C_3H_{12}O_2S$, C, 16.36; B, 49.07; S, 14.55; H, 5.49. Infrared spectra of both **A′** and **A** (measured in KBr pellets) are presented in Supporting Information Figure S12.

**Monolayer preparation.** **A** and **A′** SAMs were deposited either from solution or from the vapor phase. For solution deposition, 0.5 mmol of **A** or **A′** were dissolved in 5 mL of freshly distilled $CH_2Cl_2$ (dried with $CaH_2$) and applied to Au{111} substrates. For spectroscopic measurements of solution-deposited SAMs, two forms of gold substrates were used: Au films comprising a 200 nm thick, evaporation-deposited gold film with ∼2 nm of a Cr interlayer on a glass wafer (11 mm × 11 mm) purchased from Arrandee, Germany, and Au micrometer single crystals[19] deposited from an ethanol suspension on a quartz plate and cleaned by multiple cycles of 30 min exposure in a UV–ozone cleaner (Novascan 4″ PSD standard system) and subsequent $H_2$-flame annealing. The substrates were immersed in the respective solutions of **A** or **A′** for 1 h, then quickly removed, and immediately, before their surfaces could dry, immersed in a beaker with freshly distilled $CH_2Cl_2$ used for washing. This procedure was followed by additional rinsing with an excess of $CH_2Cl_2$ and drying in a gaseous stream of Ar.

Adsorption experiments from the gas phase were conducted on Platypus template stripped gold films (Platypus, U.S.A.). Freshly stripped gold films were exposed to vapors of either **A** or **A′** in a closed vial at room temperature.

For STM, both pure and codeposited **A** and (1:10) **A′**:**A** SAMs for STM imaging were fabricated via solution deposition onto commercially available Au{111}/mica substrates (Agilent, Santa Clara, CA). The Au/mica substrates were annealed with 10 passes of a hydrogen flame (0.5 Hz) and placed into a capped vial with 1 mL of a 1 mM solution of either **A** or **A′**:**A** (1:10) in benzene. Each sample was heated at 78 °C in a Barnstead Thermolyne 1400 furnace (ThermoFisher Scientific, Waltham, MA) for 24 h. Subsequently, samples were cleaned with neat benzene and dried with a stream of nitrogen gas before loading into the custom-built ambient microscope.

**Crystallography.** Crystals suitable for single-crystal X-ray crystallography were obtained by slow sublimation in a sealed ampule over a few weeks. The data were measured at 120 K with up to 0.87 Å resolution on an Agilent diffractometer Xcalibur using mirror-collimated Cu K$\alpha$ radiation (Gemini ultra Cu) from a sealed X-ray tube and CCD detector Atlas. Data processing was made using program CrysAlis PRO, with empirical absorption correction. Structures were solved by charge flipping with Superflip[69] and refined with Jana2006, http://jana.fzu.cz (Structure Determination Software Programs, Institute of Physics, Prague, Czech Republic).[70] The sample was a twin rotated by 180° around the reciprocal axis $c^*$. This twinning operation generated overlaps of some diffraction spots; the overlaps were detected by the data processing program CrysAlis PRO and encoded to the reflection file in a form of the so-called hklf5 format. Using this format, the partial overlaps due to twinning could be taken into account by the refinement program Jana2006. This considerably improved the sensitivity of the refinement of hydrogen atom positions.

All hydrogen atoms appeared in difference Fourier maps. Hydrogen atoms attached to boron were constrained to have the same B–H distance while hydrogen atoms attached to oxygen of carboxyl were refined with constrained O–H distances of 0.82 Å. The difference Fourier maps also revealed disorder of the thiol hydrogen, which occupied two positions, both suitable for forming S–H···S hydrogen bonds. In the refinement, the occupancy of these disordered positions was fixed to 0.5, and the distances S–H as well as the angles C–S–H were restrained to be the same. The isotropic displacement parameters of hydrogen atoms were constrained as a 1.2 multiple of the equivalent isotropic displacement parameter of their parent atoms. ORTEP-3 was used to prepare Figure 1.[71] Other figures were made in Mercury. Selected collection and refinement data are listed in Supporting Information Table S1 together with the CCDC number. Supplementary crystallographic data can be also obtained free of charge via http://www.ccdc.cam.ac.uk/conts/retrieving.html or from the Cambridge Crystallographic Data Centre, 12 Union Road, Cambridge CB2 1EZ, U.K.; fax: (+44) 1223-336-033; or e-mail: deposit@ccdc.cam.ac.uk.

**Scanning Tunneling Microscopy.** All STM measurements were performed in air using a custom beetle-style microscope and platinum/iridium probe tips (80:20).[7,72] The well-known lattice of the 1-dodecanethiolate SAM on Au{111} was used to calibrate piezoelectric scanners, and these calibrations were subsequently checked against the expected spacings of SAMs of **A**. Samples were held within a −1 to −0.1 V bias range, and 256 × 256 pixel images were collected in constant-current mode at a tunneling current of 100 pA.

**X-ray Photoelectron Spectroscopy.** Self-assembled monolayers of **A** and **A′** were measured using an ESCA310 (Scienta, Sweden) electron spectrometer equipped with a hemispherical electron analyzer operated in a fixed transmission mode. Monochromatic Al $K_\alpha$ radiation was used for electron excitation. The spectrometer was calibrated to the Au $4f_{7/2}$ peak at 84.0 eV. The spectra were recorded at room temperature. The energy spectra of the emitted Au 4f, C 1s, B 1s, and S 2p photoelectrons were measured. The electron detection angle was 45° with respect to the macroscopic sample surface. The pressure of residual gases in the analyzer chamber during spectra acquisition was $2 \times 10^{-9}$ mbar. The accuracy of the measured binding energies was ±0.1 eV. The spectra were fit after subtraction of the Shirley background[73] using Gaussian–Lorentzian line shape and nonlinear least-squares algorithms. The fitting of S 2p profiles was made subject to the constraints of the constant spin–orbit splitting 1.18 eV and the constant S $2p_{3/2}$:S $2p_{1/2}$ branching ratio 2:1.[74] Quantification of the elemental concentrations was accomplished by correcting photoelectron peak intensities for their cross sections[75] and the analyzer transmission function. In the calculations, homogeneous compositions of the analyzed layer of the samples measured was assumed. The typical error of the quantitative analysis by XPS is ∼10%.[76]

**Water Contact-Angle Measurements.** Contact angle measurements for carboranethiolate SAMs on Au/Si were performed using a custom-built goniometer. It is based on an InfiniStix (Hitachi Ltd., Tokyo, Japan) 0.50× magnification, 94 mm focal length CCD camera. Droplets are created and manipulated using a 0.5 mL Luer Lock syringe (Cole-Palmer, Vernon Hills, IL) and a 30 gauge needle. For data acquisition and contact angle measurements, FTA 1000 B software, produced by First Ten Angstroms, Inc. (Portsmouth, VA), was used.

Contact angle data were collected using a dynamic sessile drop method, where a sample is placed near the tip of the needle. A drop of deionized $H_2O$ (2 $\mu$L) is deposited on the sample, and the needle is carefully positioned in the center of the drop without deforming its shape. Drop size is then increased to 6 $\mu$L, and a photograph is obtained that provides the advancing contact angle. Drop volume is then increased to 8 $\mu$L and then reduced to 6 $\mu$L. Another photograph is obtained, resulting in the receding contact angle. All these measurements were collected on an automated system with photographs collected at 60 frames per second for seven cycles. Reported values are averages of measurements on three samples with five drops per sample.

**Computational details.** The geometries of the molecules and anions were calculated using the open-source quantum chemical package NWChem[77] with the help of the Gabedit GUI.[78] The $C_s$ symmetry of the principal rotamers was used. First, the geometries were optimized at the Hartree–Fock level in Pople's 6-31+G* basis


DOI: 10.1021/acs.chemmater.5b02263
Chem. Mater. 2015, 27, 5425–5435

that contains polarization as well as diffuse functions at all non-hydrogen atoms, the analytical Hessian of the optimized structure was calculated, and frequency analysis was performed. The number of imaginary frequencies was used to determine whether the structure is a minimum or a transition state. Finally, the geometries were further optimized at the level of the second order Møller−Plesset perturbation theory using the same basis functions set. For 1-S-12-COOH-1,12-$C_2B_{10}H_{10}$(−), conformation analysis was performed. For other species studied, possible rotamers of their carboxyl or thiol groups were tested and the most stable conformers selected.

The surface packing was modeled as a simple 2D periodic array of molecules, omitting their interactions with the metal surface. The structure was calculated within the approximations of density functional theory with plane wave basis sets using the Abinit package.[79,80] The third dimension for the 2D cell was fixed at 30 Å, while the two dimensions of interest were set to 7.2 Å, at an angle of 60°, and optimized along with the molecular geometry. The general gradient approximation exchange-correlation functional of Perdew, Burke, and Ernzerhof was used, and the atoms were described by the projector-augmented waves approximation with the atomic data downloaded from the Abinit web.[81] The plane-wave basis was cut off at the energy of 15 Ha, for the double grid cutoff 50 Ha was applied. The 3 × 3 × 1 Monkhorst−Pack *k*-point grid was automatically generated so as not to produce erroneous contributions to the Fourier transform of real space vectors shorter than 50 Å.

## ■ ASSOCIATED CONTENT

### Supporting Information

Supramolecular structure of *p*-carborane analogue of *p*-mercaptobenzoic acid (Figures S1 and S2), additional STM images of the SAM-modified Au{111} surfaces and their respective analyses (Figures S3−S5), calculated energy diagrams with the frontier orbitals visualized (Figures S6 and S7), MS and IR spectra (Figures S8−S12), X-ray crystallographic information file (CCDC 1028174), and XYZ files with the calculated atomic coordinates. The Supporting Information is available free of charge on the ACS Publications website at DOI: 10.1021/acs.chemmater.5b02263.

## ■ AUTHOR INFORMATION


### Corresponding Authors

*(Z.B.) E-mail: zdenek.bastl@jh-inst.cas.cz.
*(P.S.W.) E-mail: psw@cnsi.ucla.edu.
*(T.B.) E-mail: tbase@iic.cas.cz.


### Author Contributions

The manuscript was written through contributions of all authors. All authors have given approval to the final version of the manuscript.

### Notes

The authors declare no competing financial interest.

## ■ ACKNOWLEDGMENTS

This work was supported by the Czech Academy of Sciences (Grant No. M200321201), by the Czech Science Foundation (Grant Nos. P205-10-0348 and 14-03276S), by the Czech Ministry of Education (MSMT ERC-CZ project LL 1301), and by the Department of Energy (DE-SC-1037004) for support of the measurements and analyses. We thank Dr. Václav Šícha from the Institute of Inorganic Chemistry ASCR for the Mass Spectrometry analysis.

## ■ REFERENCES


(1) Smith, R. K.; Lewis, P. A.; Weiss, P. S. Patterning self-assembled monolayers. *Prog. Surf. Sci.* **2004**, *75*, 1−68.
(2) Kim, J.; Rim, Y. S.; Liu, Y.; Serino, A. C.; Thomas, J. C.; Chen, H.; Yang, Y.; Weiss, P. S. Interface Control in Organic Electronics Using Mixed Monolayers of Carboranethiol Isomers. *Nano Lett.* **2014**, *14*, 2946−2951.
(3) Love, J. C.; Estroff, L. A.; Kriebel, J. K.; Nuzzo, R. G.; Whitesides, G. M. Self-assembled monolayers of thiolates on metals as a form of nanotechnology. *Chem. Rev.* **2005**, *105*, 1103−1169.
(4) Gooding, J. J.; Ciampi, S. The molecular level modification of surfaces: from self-assembled monolayers to complex molecular assemblies. *Chem. Soc. Rev.* **2011**, *40*, 2704−2718.
(5) Ulman, A. Formation and structure of self-assembled monolayers. *Chem. Rev.* **1996**, *96*, 1533−1554.
(6) Fujii, S.; Akiba, U.; Fujihira, M. Geometry for self-assembling of spherical hydrocarbon cages with methane thiolates on Au(111). *J. Am. Chem. Soc.* **2002**, *124*, 13629−13635.
(7) Hohman, J. N.; Claridge, S. A.; Kim, M.; Weiss, P. S. Cage molecules for self-assembly. *Mater. Sci. Eng., R* **2010**, *70*, 188−208.
(8) von Wrochem, F.; Scholz, F.; Gao, D.; Nothofer, H.-G.; Yasuda, A.; Wessels, J. M.; Roy, S.; Chen, X.; Michl, J. High-Band-Gap Polycrystalline Monolayers of a 12-Vertex *p*-Carborane on Au(111). *J. Phys. Chem. Lett.* **2010**, *1*, 3471−3477.
(9) Hohman, J. N.; Kim, M.; Schüpbach, B.; Kind, M.; Thomas, J. C.; Terfort, A.; Weiss, P. S. Dynamic Double Lattice of 1-Adamantaneselenolate Self-Assembled Monolayers on Au{111}. *J. Am. Chem. Soc.* **2011**, *133*, 19422−19431.
(10) Spokoyny, A. M.; Machan, C. W.; Clingerman, D. J.; Rosen, M. S.; Wiester, M. J.; Kennedy, R. D.; Stern, C. L.; Sarjeant, A. A.; Mirkin, C. A. A coordination chemistry dichotomy for icosahedral carborane-based ligands. *Nat. Chem.* **2011**, *3*, 590−596.
(11) Katano, S.; Kim, Y.; Kitagawa, T.; Kawai, M. Tailoring electronic states of a single molecule using adamantane-based molecular tripods. *Phys. Chem. Chem. Phys.* **2013**, *15*, 14229−14233.
(12) Wann, D. A.; Lane, P. D.; Robertson, H. E.; Baše, T.; Hnyk, D. The gaseous structure of *closo*-9,12-$(SH)_2$-1,2-$C_2B_{10}H_{10}$, a modifier of gold surfaces, as determined using electron diffraction and computational methods. *Dalton Trans.* **2013**, *42*, 12015−12019.
(13) Grimes, R. N. Carboranes in the chemist's toolbox. *Dalton Trans.* **2015**, *44*, 5939−5956.
(14) Yeager, L. J.; Saeki, F.; Shelly, K.; Hawthorne, M. F.; Garrell, R. A new class of self-assembled monolayers: *closo*-$B_{12}H_{11}S_3$- on gold. *J. Am. Chem. Soc.* **1998**, *120*, 9961−9962.
(15) Scholz, F.; Nothofer, H.-G.; Wessels, J. M.; Nelles, G.; von Wrochem, F.; Roy, S.; Chen, X.; Michl, J. Permethylated 12-Vertex *p*-Carborane Self-Assembled Monolayers. *J. Phys. Chem. C* **2011**, *115*, 22998−23007.
(16) Claridge, S. A.; Liao, W. S.; Thomas, J. C.; Cao, H.; Cheunkar, S.; Serino, A. C.; Andrews, A. M.; Weiss, P. S.; Zhao, Y. From the bottom up: dimensional control and characterization in molecular monolayers. *Chem. Soc. Rev.* **2013**, *42*, 2725−2745.
(17) Baše, T.; Bastl, Z.; Plzák, Z.; Grygar, T.; Plešek, J.; Carr, M. J.; Malina, V.; Šubrt, J.; Boháček, J.; Večerníková, E.; Kříž, O. Carboranethiol-modified gold surfaces. A study and comparison of modified cluster and flat surfaces. *Langmuir* **2005**, *21*, 7776−7785.
(18) Hohman, J. N.; Zhang, P. P.; Morin, E. I.; Han, P.; Kim, M.; Kurland, A. R.; McClanahan, P. D.; Balema, V. P.; Weiss, P. S. Self-Assembly of Carboranethiol Isomers on Au{111}: Intermolecular Interactions Determined by Molecular Dipole Orientations. *ACS Nano* **2009**, *3*, 527−536.
(19) Baše, T.; Bastl, Z.; Šlouf, M.; Klementová, M.; Šubrt, J.; Vetushka, A.; Ledinský, M.; Fejfar, A.; Macháček, J.; Carr, M. J.; Londesborough, M. G. S. Gold micrometer crystals modified with carboranethiol derivatives. *J. Phys. Chem. C* **2008**, *112*, 14446−14455.
(20) Baše, T.; Bastl, Z.; Hávranek, V.; Lang, K.; Bould, J.; Londesborough, M. G. S.; Macháček, J.; Plešek, J. Carborane-thiol-silver interactions. A comparative study of the molecular protection of silver surfaces. *Surf. Coat. Technol.* **2010**, *204*, 2639−2646.
(21) Lübben, J. F.; Baše, T.; Rupper, P.; Künniger, T.; Macháček, J.; Guimond, S. Tuning the surface potential of Ag surfaces by




DOI: 10.1021/acs.chemmater.5b02263
*Chem. Mater.* 2015, 27, 5425−5435

chemisorption of oppositely-oriented thiolated carborane dipoles. *J. Colloid Interface Sci.* **2011**, *354*, 168−174.
(22) Ito, M.; Wei, T. X.; Chen, P.-L.; Akiyama, H.; Matsumoto, M.; Tamada, K.; Yamamoto, Y. A novel method for creation of free volume in a one-component self-assembled monolayer. Dramatic size effect of *para*-carborane. *J. Mater. Chem.* **2005**, *15*, 478−483.
(23) Langecker, J.; Fejfarová, K.; Dušek, M.; Rentsch, D.; Baše, T. Carbon-substituted 9,12-dimercapto-1,2-dicarba-*closo*-dodecaboranes via a 9,12-*bis*(methoxy-methylthio)-1,2-dicarba-*closo*-dodecaborane precursor. *Polyhedron* **2012**, *45*, 144−151.
(24) Frank, R.; Boehnke, S.; Aliev, A.; Hey-Hawkins, E. From *ortho*-carbaborane-9-thiol towards new building blocks. *Polyhedron* **2012**, *39*, 9−13.
(25) Kabytaev, K. Z.; Everett, T. A.; Safronov, A. V.; Sevryugina, Y. V.; Jalisatgi, S. S.; Hawthorne, M. F. B-Mercaptocarboranes: A New Synthetic Route. *Eur. J. Inorg. Chem.* **2013**, *2013*, 2488−2491.
(26) Weiss, P. S. Functional Molecules and Assemblies in Controlled Environments: Formation and Measurements. *Acc. Chem. Res.* **2008**, *41*, 1772−1781.
(27) Ackerson, C. J.; Jadzinsky, P. D.; Kornberg, R. D. Thiolate ligands for synthesis of water-soluble gold clusters. *J. Am. Chem. Soc.* **2005**, *127*, 6550−6551.
(28) Jadzinsky, P. D.; Calero, G.; Ackerson, C. J.; Bushnell, D. A.; Kornberg, R. D. Structure of a thiol monolayer-protected gold nanoparticle at 1.1 Ångstrom resolution. *Science* **2007**, *318*, 430−433.
(29) Walter, M.; Akola, J.; Lopez-Acevedo, O.; Jadzinsky, P. D.; Calero, G.; Ackerson, C. J.; Whetten, R. L.; Grönbeck, H.; Häkkinen, H. A unified view of ligand-protected gold clusters as superatom complexes. *Proc. Natl. Acad. Sci. U. S. A.* **2008**, *105*, 9157−9162.
(30) Saavedra, H. M.; Thompson, C. M.; Hohman, J. N.; Crespi, V. H.; Weiss, P. S. Reversible Lability by in Situ Reaction of Self-Assembled Monolayers. *J. Am. Chem. Soc.* **2009**, *131*, 2252−2259.
(31) Saavedra, H. M.; Mullen, T. J.; Zhang, P. P.; Dewey, D. C.; Claridge, S. A.; Weiss, P. S. Hybrid strategies in nanolithography. *Rep. Prog. Phys.* **2010**, *73*, 036501.
(32) Davidson, M. G.; Hibbert, T. G.; Howard, J. A. K.; Mackinnon, A.; Wade, K. Definitive crystal structures of *ortho*-, *meta*- and *para*-carboranes: Supramolecular structures directed solely by C-H•••O hydrogen bonding to hmpa (hmpa = hexamethylphosphoramide). *Chem. Commun.* **1996**, *19*, 2285−2286.
(33) Tiritiris, I.; Schleid, T. Z. The dodecahydro-*closo*-dodecaborates $M_2[B_{12}H_{12}]$ of the heavy alkali metals ($M = K^+$, $Rb^+$, $NH_4^+$, $Cs^+$) and their formal iodide adducts $M_3I[B_{12}H_{12}]$ ($MI•M_2[B_{12}H_{12}]$). *Z. Anorg. Allg. Chem.* **2003**, *629*, 1390−1402.
(34) Hnyk, D.; Holub, J.; Hofmann, M.; van Rague Schleyer, P.; Robertson, H. E.; Rankin, D. W. H. Synthesis and molecular structure of 1,12-dicarba-*closo*-dodecaborane(12)-1,12-dithiol, 1,12-$(SH)_2$-1,12-$C_2B_{10}H_{10}$, in the gaseous phase, determined by electron diffraction and ab initio calculations; geometrical consequences of three-dimensional aromaticity in carbaboranes 1,12-$X_2$−1,12-$C_2B_{10}H_{10}$. *J. Chem. Soc., Dalton Trans.* **2000**, 4617−4622.
(35) Bernstein, J.; Davis, R. E.; Shimoni, L.; Chang, N.-L. Patterns in Hydrogen Bonding: Functionality and Graph Set Analysis in Crystals. *Angew. Chem., Int. Ed. Engl.* **1995**, *34*, 1555−1573.
(36) Claridge, S. A.; Schwartz, J. J.; Weiss, P. S. Electrons, Photons, and Force: Quantitative Single-Molecule Measurements from Physics to Biology. *ACS Nano* **2011**, *5*, 693−729.
(37) Hohman, J. N.; Thomas, J. C.; Zhao, Y.; Auluck, H.; Kim, M.; Vijselaar, W. J. C.; Kommeren, S.; Terfort, A.; Weiss, P. S. Exchange Reactions between Alkanethiolates and Alkaneselenols on Au{111}. *J. Am. Chem. Soc.* **2014**, *136*, 8110−8121.
(38) Han, P.; Kurland, A. R.; Giordano, A. N.; Nanayakkara, S. U.; Blake, M. M.; Pochas, C. M.; Weiss, P. S. Heads and Tails: Simultaneous Exposed and Buried Interface Imaging of Monolayers. *ACS Nano* **2009**, *3*, 3115−3121.
(39) Claridge, S. A.; Thomas, J. C.; Silverman, M. A.; Schwartz, J. J.; Yang, Y.; Wang, C.; Weiss, P. S. Differentiating Amino Acid Residues and Side Chain Orientations in Peptides Using Scanning Tunneling Microscopy. *J. Am. Chem. Soc.* **2013**, *135*, 18528−18535.
(40) Fujii, S.; Akiba, U.; Fujihira, M. Geometry for self-assembling of spherical hydrocarbon cages with methane thiolates on Au(111). *J. Am. Chem. Soc.* **2002**, *124*, 13629−13635.
(41) Farha, O.; Spokoyny, A. M.; Mulfort, K. L.; Hawthorne, M. F.; Mirkin, C. A.; Hupp, J. T. Synthesis and hydrogen sorption properties of carborane based metal-organic framework materials. *J. Am. Chem. Soc.* **2007**, *129*, 12680−12681.
(42) Stranick, S. J.; Parikh, A. N.; Tao, Y.-T.; Allara, D. L.; Weiss, P. S. Phase-separation of mixed-composition self-assembled monolayers into nanometer-scale molecular domains. *J. Phys. Chem.* **1994**, *98*, 7636−7646.
(43) Weck, M.; Jackiw, J. J.; Rossi, R. R.; Weiss, P. S.; Grubbs, R. H. Ring-opening metathesis polymerization from surfaces. *J. Am. Chem. Soc.* **1999**, *121*, 4088−4089.
(44) Liu, G.-Y.; Xu, S.; Qian, Y. Nanofabrication of self-assembled monolayers using scanning probe lithography. *Acc. Chem. Res.* **2000**, *33*, 457−466.
(45) Zhang, H.; Li, Z.; Mirkin, C. A. Dip-pen nanolithography-based methodology for preparing arrays of nanostructures functionalized with oligonucleotides. *Adv. Mater.* **2002**, *14*, 1472−1473.
(46) Srinivasan, C.; Mullen, T. J.; Hohman, J. N.; Anderson, M. E.; Dameron, A. A.; Andrews, A. M.; Dickey, E. C.; Horn, M. W.; Weiss, P. S. Scanning electron microscopy of nanoscale chemical patterns. *ACS Nano* **2007**, *1*, 191−201.
(47) Mullen, T. J.; Srinivasan, C.; Hohman, J. N.; Gillmor, S. D.; Shuster, M. J.; Horn, M. W.; Andrews, A. M.; Weiss, P. S. Microcontact insertion printing. *Appl. Phys. Lett.* **2007**, *90*, 063114.
(48) Shuster, M. J.; Vaish, A.; Szapacs, M. E.; Anderson, M. E.; Weiss, P. S.; Andrews, A. M. Biospecific recognition of tethered small molecules diluted is self-assembled monolayers. *Adv. Mater.* **2008**, *20*, 164−167.
(49) Spokoyny, A. M.; Kim, D.; Sumrein, A.; Mirkin, C. A. Infinite coordination polymer nano- and microparticle structures. *Chem. Soc. Rev.* **2009**, *38*, 1218−1227.
(50) Liao, W.-S.; Cheunkar, S.; Cao, H.; Bednar, H.; Weiss, P. S.; Andrews, A. M. Subtractive Patterning via Chemical Lift-Off Lithography. *Science* **2012**, *337*, 1517−1521.
(51) Zheng, Y. B.; Pathem, B. K.; Hohman, J. N.; Thomas, J. C.; Kim, M. H.; Weiss, P. S. Photoresponsive Molecules in Well-Defined Nanoscale Environments. *Adv. Mater.* **2013**, *25*, 302−312.
(52) Castner, D. G.; Hinds, K.; Grainger, D. W. X-ray photoelectron spectroscopy sulfur 2p study of organic thiol and disulfide binding interactions with gold surfaces. *Langmuir* **1996**, *12*, 5083−5086.
(53) Duwez, A.-S. Exploiting electron spectroscopies to probe the structure and organization of self-assembled monolayers: a review. *J. Electron Spectrosc. Relat. Phenom.* **2004**, *134*, 97−138.
(54) Pensa, E.; Cortés, E.; Corthey, G.; Carro, P.; Vericat, C.; Fonticelli, M. H.; Benítez, G.; Rubert, A. A.; Salvarezza, R. C. The Chemistry of the Sulfur-Gold Interface: In Search of a Unified Model. *Acc. Chem. Res.* **2012**, *45*, 1183−1192.
(55) Yu, M.; Bovet, N.; Satterley, C. J.; Bengió, S.; Lovelock, K. R. J.; Milligan, P. K.; Jones, R. G.; Woodruff, D. P.; Dhanak, V. True nature of an archetypal self-assembly system: Mobile Au-thiolate species on Au(111). *Phys. Rev. Lett.* **2006**, *97*, 166102.
(56) Maksymovych, P.; Sorescu, D. C.; Yates, J. T., Jr. Gold-adatom-mediated bonding in self-assembled short-chain alkanethiolate species on the Au(111) surface. *Phys. Rev. Lett.* **2006**, *97*, 146103.
(57) Moore, A. M.; Mantooth, B. A.; Donhauser, Z. J.; Yao, Y.; Tour, J. M.; Weiss, P. S. Real-time measurements of conductance switching and motion of single oligo(phenylene ethynylene) molecules. *J. Am. Chem. Soc.* **2007**, *129*, 10352−10353.
(58) Jadzinsky, P. D.; Calero, G.; Ackerson, C. J.; Bushnell, D. A.; Kornberg, R. D. Structure of a thiol monolayer-protected gold nanoparticle at 1.1 Ångstrom resolution. *Science* **2007**, *318*, 430−433.
(59) Maksymovych, P.; Voznyy, O.; Dougherty, D. B.; Sorescu, D. C.; Yates, J. T., Jr. Gold adatom as a key structural component in self-assembled monolayers of organosulfur molecules on Au(111). *Prog. Surf. Sci.* **2010**, *85*, 206−240.


DOI: 10.1021/acs.chemmater.5b02263
*Chem. Mater.* 2015, 27, 5425−5435

(60) Vericat, C.; Vela, M. E.; Benitez, G.; Carro, P.; Salvarezza, R. C. Self-assembled monolayers of thiols and dithiols on gold: new challenges for a well-known system. *Chem. Soc. Rev.* **2010**, *39*, 1805−1834.
(61) Poirier, G. E. Characterization of organosulfur molecular monolayers on Au(111) using scanning tunneling microscopy. *Chem. Rev.* **1997**, *97*, 1117−1127.
(62) Donhauser, Z. J.; Price, D. W., Jr.; Tour, J. M.; Weiss, P. S. Control of alkanethiolate monolayer structure using vapor-phase annealing. *J. Am. Chem. Soc.* **2003**, *125*, 11462−11463.
(63) Vaish, A.; Shuster, M. J.; Cheunkar, S.; Weiss, P. S.; Andrews, A. M. Tuning Stamp Surface Energy for Soft Lithography of Polar Molecules to Fabricate Bioactive Small-Molecule Microarrays. *Small* **2011**, *7*, 1471−1479.
(64) Fujita, K.; Nakamura, N.; Ohno, H.; Leigh, B. S.; Niki, K.; Gray, H. B.; Richards, J. H. Mimicking protein-protein electron transfer: Voltammetry of *Pseudomonas aeruginosa* azurin and the *Thermus thermophilus* $Cu_A$ domain at $\omega$-derivatized self-assembled-monolayer gold electrodes. *J. Am. Chem. Soc.* **2004**, *126*, 13954−13961.
(65) Thomas, J. C.; Schwartz, J. J.; Hohman, J. N.; Claridge, S. A.; Auluck, H. S.; Serino, A. C.; Spokoyny, A. M.; Tran, G.; Kelly, K. F.; Mirkin, C. A.; Gilles, J.; Osher, S. J.; Weiss, P. S. Defect-tolerant aligned dipoles within two-dimensional plastic lattices. *ACS Nano* **2015**, *9*, 4734.
(66) Plešek, J.; Heřmánek, S. Experimental evaluation of charge-distribution on particular skeletal atoms in icosahedral carboranes by means of HS-derivatives. *Collect. Czech. Chem. Commun.* **1979**, *44*, 24−33.
(67) Plešek, J.; Heřmánek, S. Syntheses and properties of substituted icosahedral carborane thiols. *Collect. Czech. Chem. Commun.* **1981**, *46*, 687−692.
(68) Baše, T.; Bastl, Z.; Havránek, V.; Macháček, J.; Langecker, J.; Malina, V. Carboranedithiols: Building Blocks for Self-Assembled Monolayers on Copper Surfaces. *Langmuir* **2012**, *28*, 12518−12526.
(69) Palatinus, L.; Chapuis, G. SUPERFLIP - a computer program for the solution of crystal structures by charge flipping in arbitrary dimensions. *J. Appl. Crystallogr.* **2007**, *40*, 786−790.
(70) Petříček, V.; Dušek, M.; Palatinus, L. Crystallographic Computing System JANA2006: General features. *Z. Kristallogr. - Cryst. Mater.* **2014**, *229*, 345−352.
(71) Farrugia, L. J. *ORTEP*-3 for Windows - a version of *ORTEP*-III with a Graphical User Interface (GUI). *J. Appl. Crystallogr.* **1997**, *30*, 565−565.
(72) Bumm, L. A.; Arnold, J. J.; Charles, L. F.; Dunbar, T. D.; Allara, D. L.; Weiss, P. S. Directed self-assembly to create molecular terraces with molecularly sharp boundaries in organic monolayers. *J. Am. Chem. Soc.* **1999**, *121*, 8017−8021.
(73) Shirley, D. A. High-resolution X-ray photoemission spectrum of valence bands of gold. *Phys. Rev. B* **1972**, *5*, 4709−4714.
(74) Moulder, J. F.; Stickle, W. F.; Sobol, P. E.; Bomben, K. D. *Handbook of X-ray Photoelectron Spectroscopy*; Perkin-Elmer Corp.: Eden Prairie, MN, 1992; p 60.
(75) Scofield, J. H. Hartree-Slater subshell photoionization cross-sections at 1254 and 1487 eV. *J. Electron Spectrosc. Relat. Phenom.* **1976**, *8*, 129−137.
(76) Briggs, D., Grant, J. T., Ed. *Surface Analysis by Auger and X-Ray Photoelectron Spectroscopy*; IM Publications and SurfaceSpectra Ltd., Cromwell Press: Trowbridge, 2003; p 326.
(77) Valiev, M.; Bylaska, E. J.; Govind, N.; Kowalski, K.; Straatsma, T. P.; Van Dam, H. J. J.; Wang, D.; Nieplocha, J.; Apra, E.; Windus, T. L.; de Jong, W. A. NWChem: A comprehensive and scalable open-source solution for large scale molecular simulations. *Comp. Phys. Comput. Phys. Commun.* **2010**, *181*, 1477−1489.
(78) Allouche, A.-R. Gabedit − A graphical user interface for computational chemistry softwares. *J. Comput. Chem.* **2011**, *32*, 174−182.
(79) *ABINIT*; Université Catholique de Louvain, Corning Incorporated, Université de Liège, Commissariat à l'Energie Atomique, Mitsubishi Chemical Corp., Ecole Polytechnique Palaiseau, and other contributors. http://www.abinit.org.
(80) Gonze, X.; Amadon, B.; Anglade, P.-M.; Beuken, J.-M.; Bottin, F.; Boulanger, P.; Bruneval, F.; Caliste, D.; Caracas, R.; Cote, M.; Deutsch, T.; Genovese, L.; Ghosez, P.; Giantomassi, M.; Goedecker, S.; Hamann, D. R.; Hermet, P.; Jollet, F.; Jomard, G.; Leroux, S.; Mancini, M.; Mazevet, S.; Oliveira, M. J. T.; Onida, G.; Pouillon, Y.; Rangel, T.; Rignanese, G.-M.; Sangalli, D.; Shaltaf, R.; Torrent, M.; Verstraete, M. J.; Zerah, G.; Zwanziger, J. W. ABINIT: First-principles approach to material and nanosystem properties. *Comput. Phys. Commun.* **2009**, *180*, 2582−2615.
(81) PAW dataset for Abinit — ABINIT. http://www.abinit.org/downloads/PAW2 (accessed Jan. 2014).


DOI: 10.1021/acs.chemmater.5b02263
*Chem. Mater.* 2015, 27, 5425−5435